# Electronic Supplementary Information

## 3D porous spheroidal $Na_4Mn_{0.9}Ce_{0.1}V(PO_4)_3$@$CeO_2$/C cathode for high-energy Na ion batteries

Kun Wang[a], Xiaobing Huang[b,*], Tao Zhou[a,*], Dan Sun[a], Haiyan Wang[a,*], Zhi Zhang[b]

[a]*Hunan Provincial Key Laboratory of Chemical Power Sources, College of Chemistry and Chemical Engineering, Central South University, Changsha 410083, China*

[b]*Hunan Provincial Key Laboratory of Water Treatment Functional Materials, Hunan Provincial Key Laboratory for Control Technology of Distributed Electric Propulsion Aircraf, College of Chemistry and Materials Engineering, Hunan University of Arts and Science, Changde 415000, China*

* Corresponding authors:
E-mail address:hxb220170@126.com (X. B. Huang), zhoutao@csu.edu.cn(T. Zhou) , wanghy419@csu.edu.cn (H. Wang)

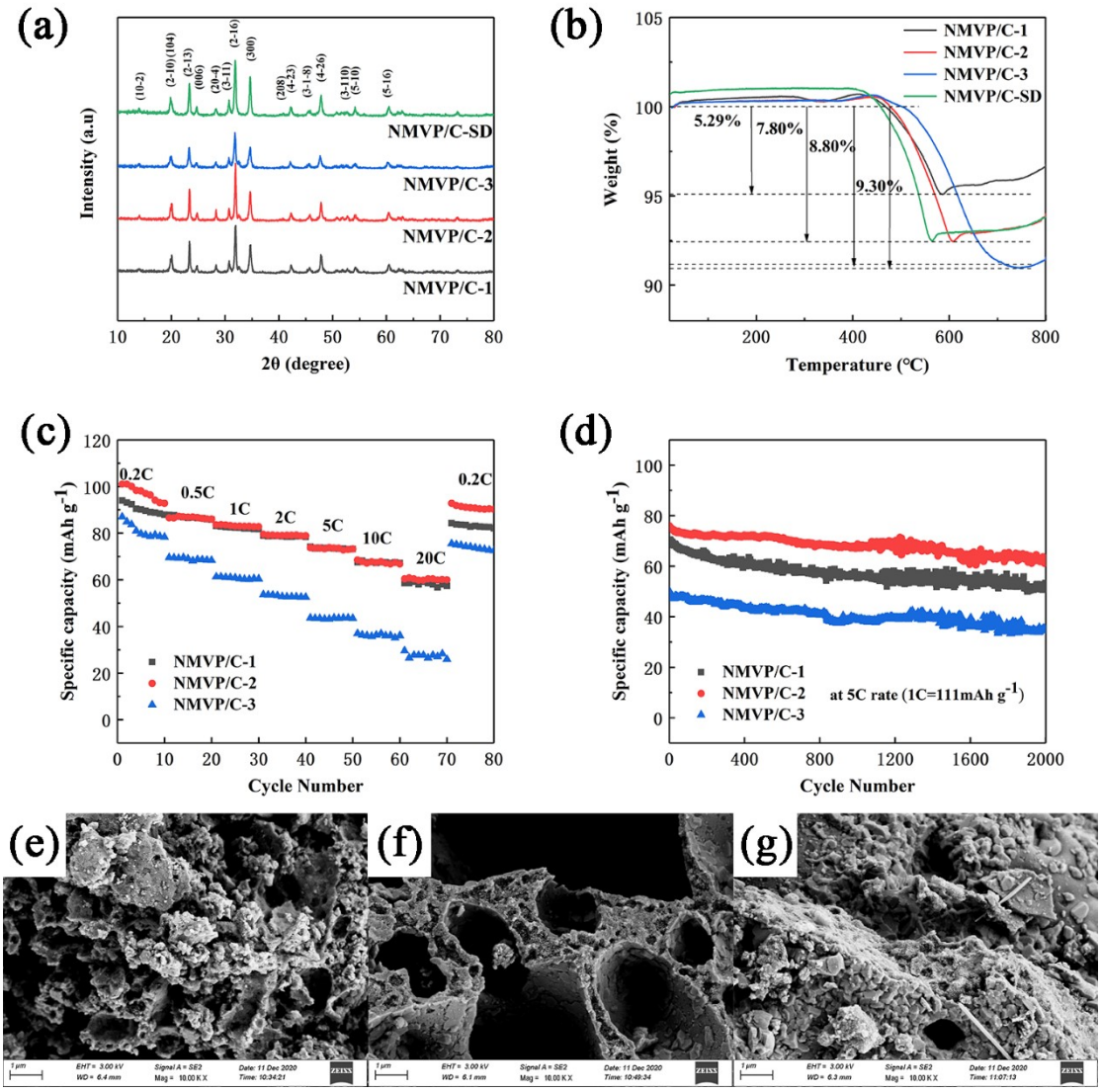


**Figure S1** (a) XRD patterns and (b) TG curves of NMVP/C samples prepared through sample sol-gel method and NMVP/C-SD sample obtained via spray-drying assisted method; (c, d) The rate and cycling performances of NMVP/C; SEM patterns of (e) NMVP/C-1, (f) NMVP/C-2 and (g) NMVP/C-3.

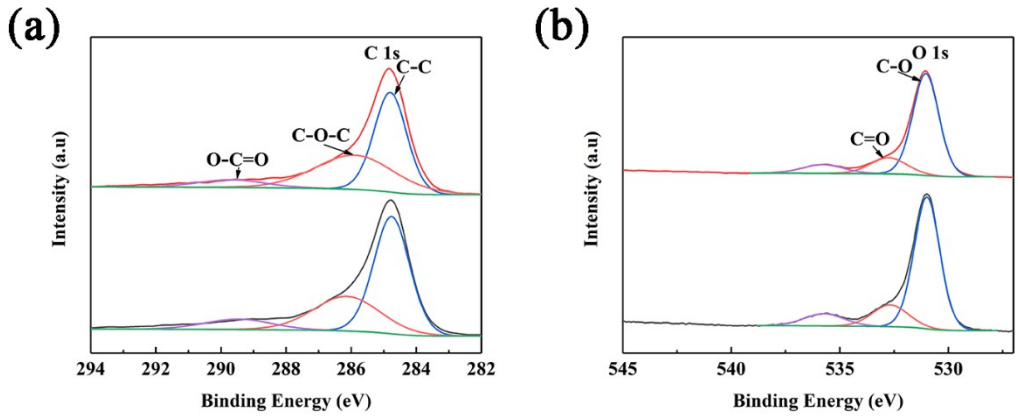


**Figure S2** A high-resolution XPS spectrum of (a) C 1s and (b) O 1s in $Na_4Mn_{1-x}Ce_xV(PO_4)_3/C$ (x = 0 and 0.1) samples.

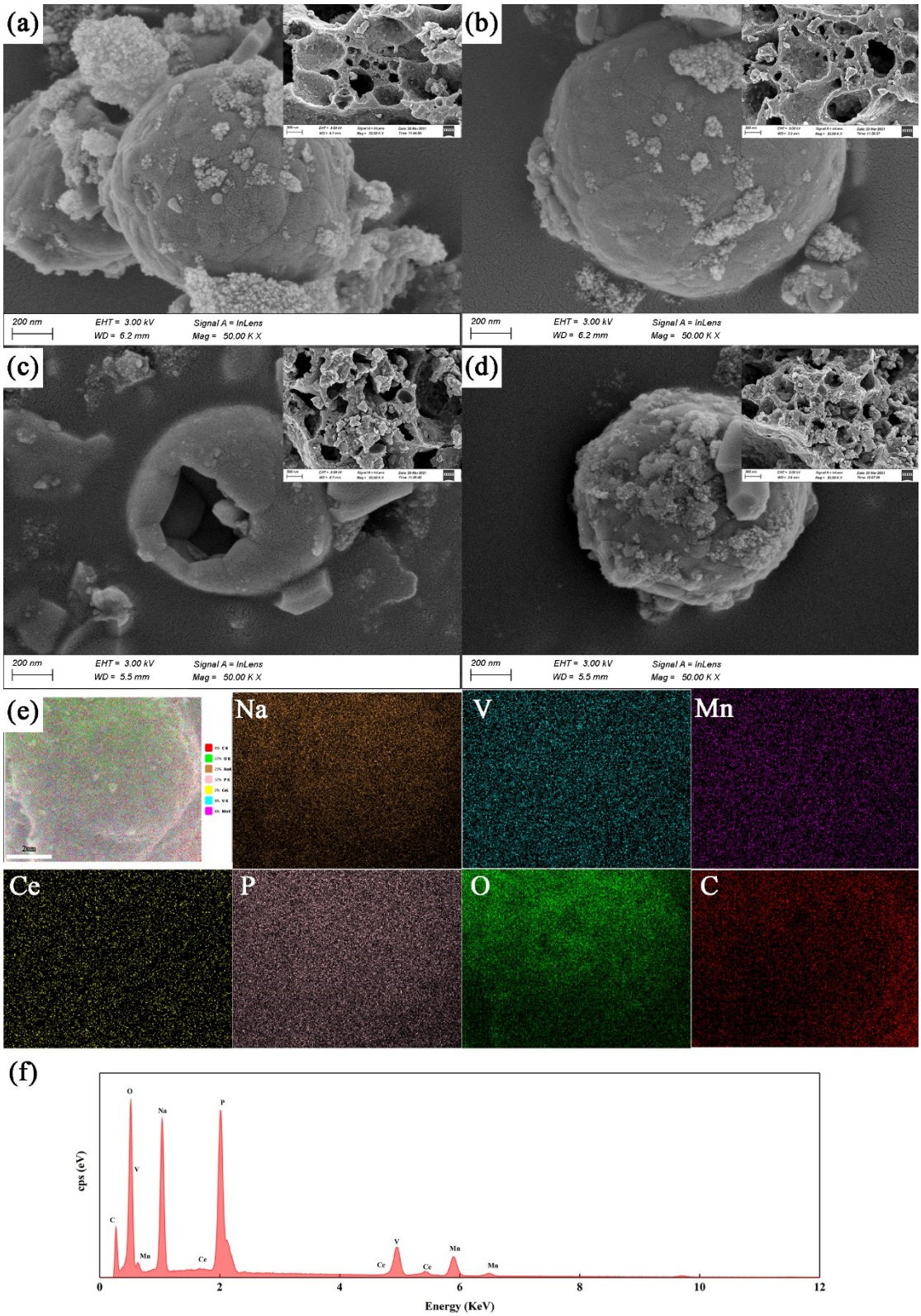


**Figure S3** SEM images of $Na_4Mn_{1-x}Ce_xV(PO_4)_3/C$ samples when (a) x = 0, (b) x = 0.05, (c) x=0.1 and (d) x=0.15**;** EDS (d) mapping images and (f) selected area of $Na_4Mn_{0.9}Ce_{0.1}V(PO_4)_3/C$ composite.

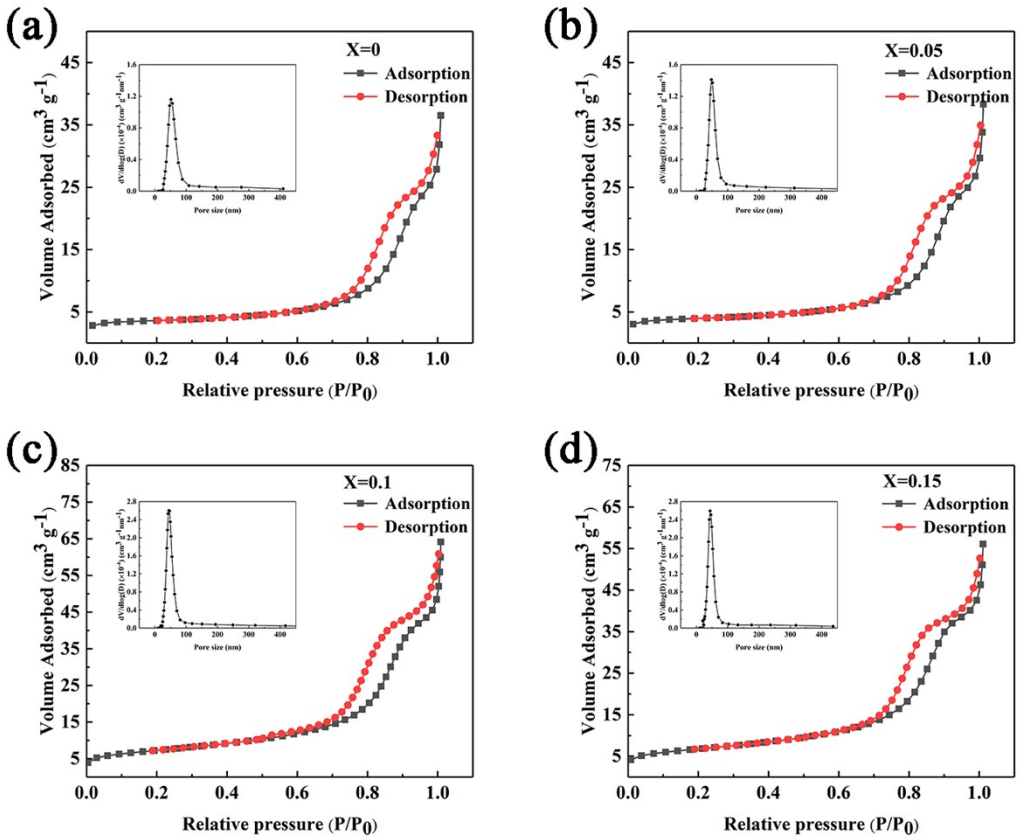


**Figure S4** $N_2$ adsorption/desorption isotherms of $Na_4Mn_{1-x}Ce_xV(PO_4)_3/C$ samples when (a) x = 0, (b) x = 0.05, (c) x=0.1 and (d) x=0.15; The inset shows their pore size distributions

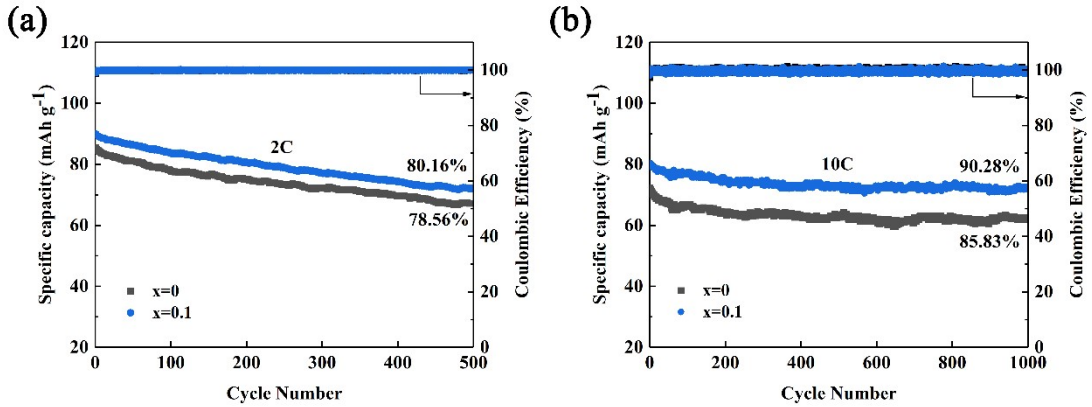


**Figure S5** Cycling stability for $Na_4Mn_{1-x}Ce_xV(PO_4)_3/C$ (x = 0 and 0.1) at (a) 2 C and (b) 10 C.

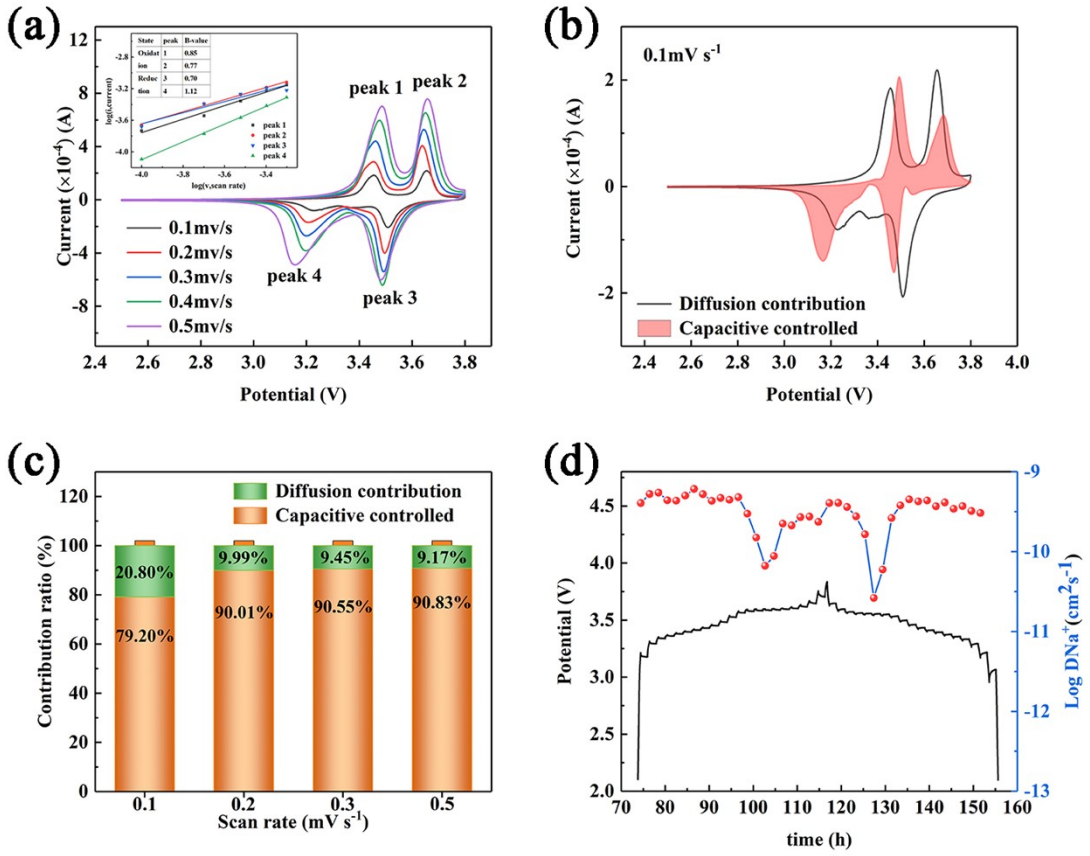


**Figure S6** (a) CV curves of $Na_4Mn_{0.9}Ce_{0.1}V(PO_4)_3$/C cathode at different scan rate, the inset is the relationship curve between log (i) and log at four peaks; (b) The calculated capacitance contribution (red region) of $Na_4Mn_{0.9}Ce_{0.1}V(PO_4)_3$/C sample at 0.1mV $s^{-1}$; (c) The capacitance contribution (orange region) for $Na_4Mn_{0.9}Ce_{0.1}V(PO_4)_3$/C cathode at series scan rates; (d) GITT profile and calculated Log ($D_{Na^+}$) for $Na_4Mn_{0.9}Ce_{0.1}V(PO_4)_3$/C cathode.

The quantitative study of pseudocapacitive contributions in electrode materials is operated by using the following equations[1]:

$$i_p = av^b \qquad \text{(S1)}$$

$$\log(i_p) = b \times \log(v) + \log a \qquad \text{(S2)}$$

$$i(V)/v^{1/2} = k_1 v^{1/2} + k_2 \qquad \text{(S3)}$$

Where v and i corresponds to scan rate and peak current,respectively.the parameters of a, b and k are adjustable constants, in which b take a value between 0.5 (diffusion limited reaction) and 1 (surface-dominated capacitive process).

Besides, galvanostatic intermittent titration technique (GITT) analysis was accomplished for $Na_4Mn_{0.9}Ce_{0.1}V(PO_4)_3$/C electrode in the working voltage region of 2.5~3.8V during second cycle, with a relaxed time of 1.5h and charging time of 0.5h. The calculation equation for the $Na^+$ diffusion coefficient can rely on Fick's second law[2], as following:

$$D = \frac{4}{\pi\tau}\left(\frac{m_B V_m}{M_B S}\right)^2\left(\frac{\Delta E_s}{\Delta E_\tau}\right)^2 \qquad \text{(S4)}$$

Where τ, mB, $M_B$, $V_m$ and S represent the current pulse time, total mass of active material, molecular weight, molar volume and surface area. The $\Delta E_s$ and $\Delta E_\tau$ correspond to the variation of steady-state voltage and total voltage change during a constant pulse.

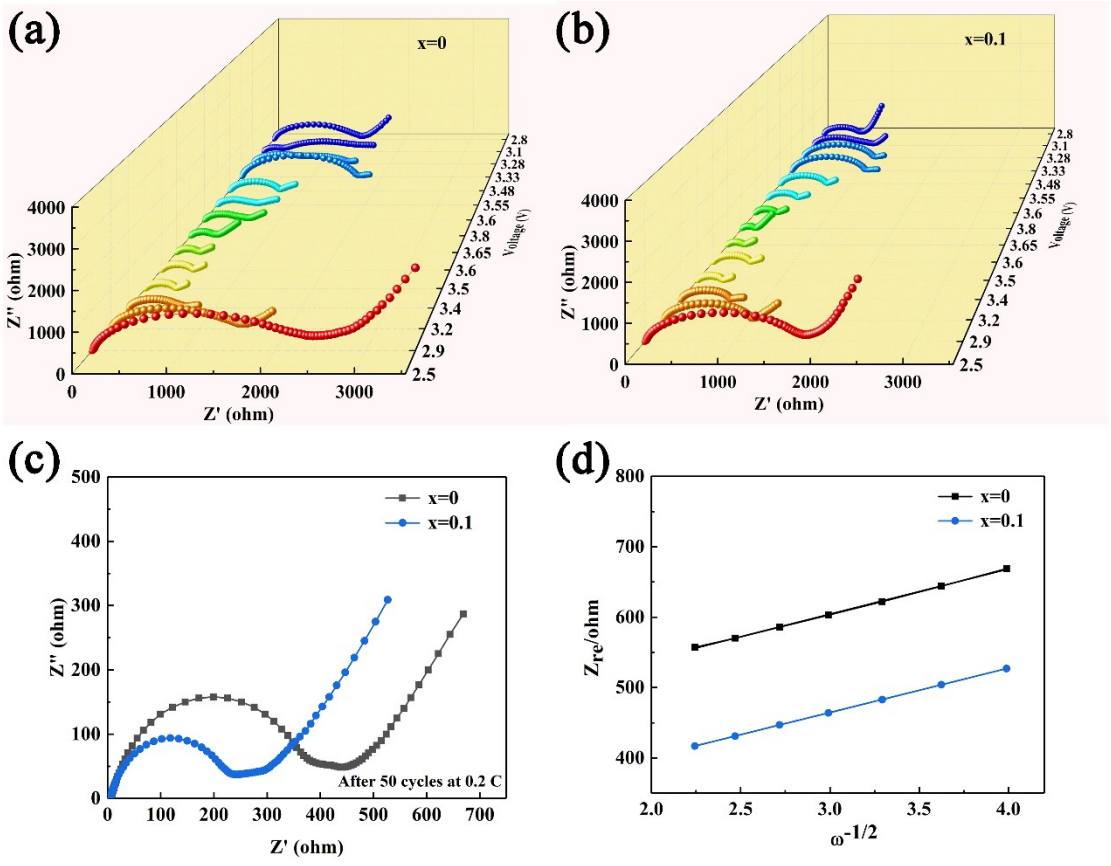


**Figure S7** Nyquist plots for the electrodes made of (a) $Na_4MnV(PO_4)_3$/C and (b) $Na_4Mn_{0.9}Ce_{0.1}V(PO_4)_3$/C during cycling test, respectively; (c) Nyquist plots and (f) the relation curves of Z′ vs. $\omega^{-1/2}$ for $Na_4Mn_{1-x}Ce_xV(PO_4)_3$/C (x = 0 and 0.1) electrodes after 50 cycles at 0.2 C.

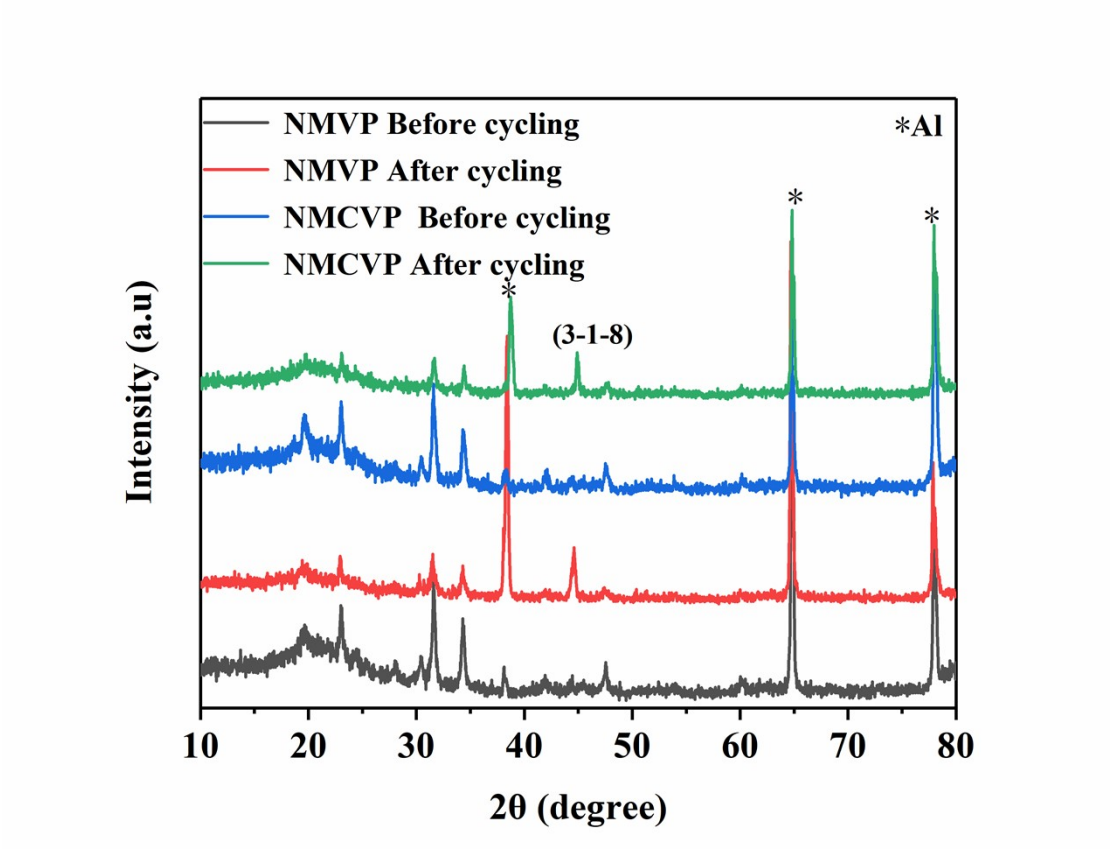


**Figure S8** XRD patterns of the $Na_4Mn_{1-x}Ce_xV(PO_4)_3/C$ (x = 0 and 0.1) electrodes before cycling and after 50 cycles at 5 C.

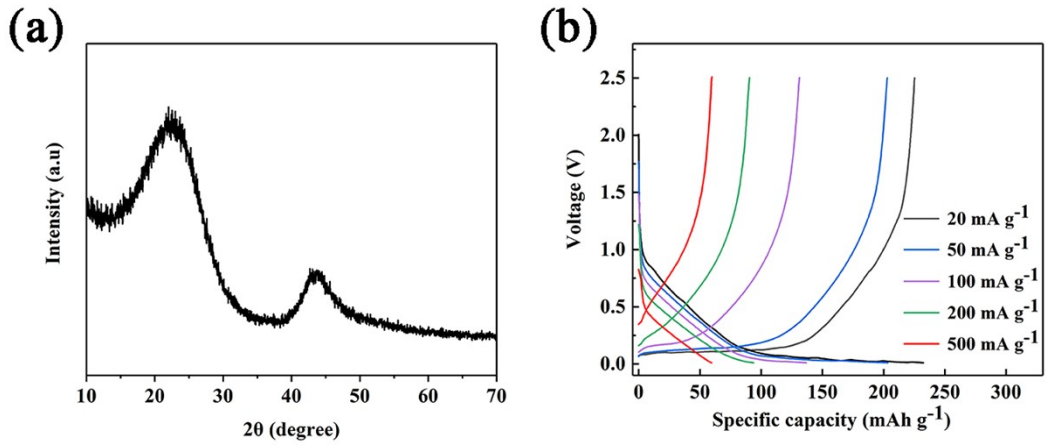


**Figure S9** (a) XRD patterns of CHC; (b) Charge and discharge curves of CHC anode in half cell.

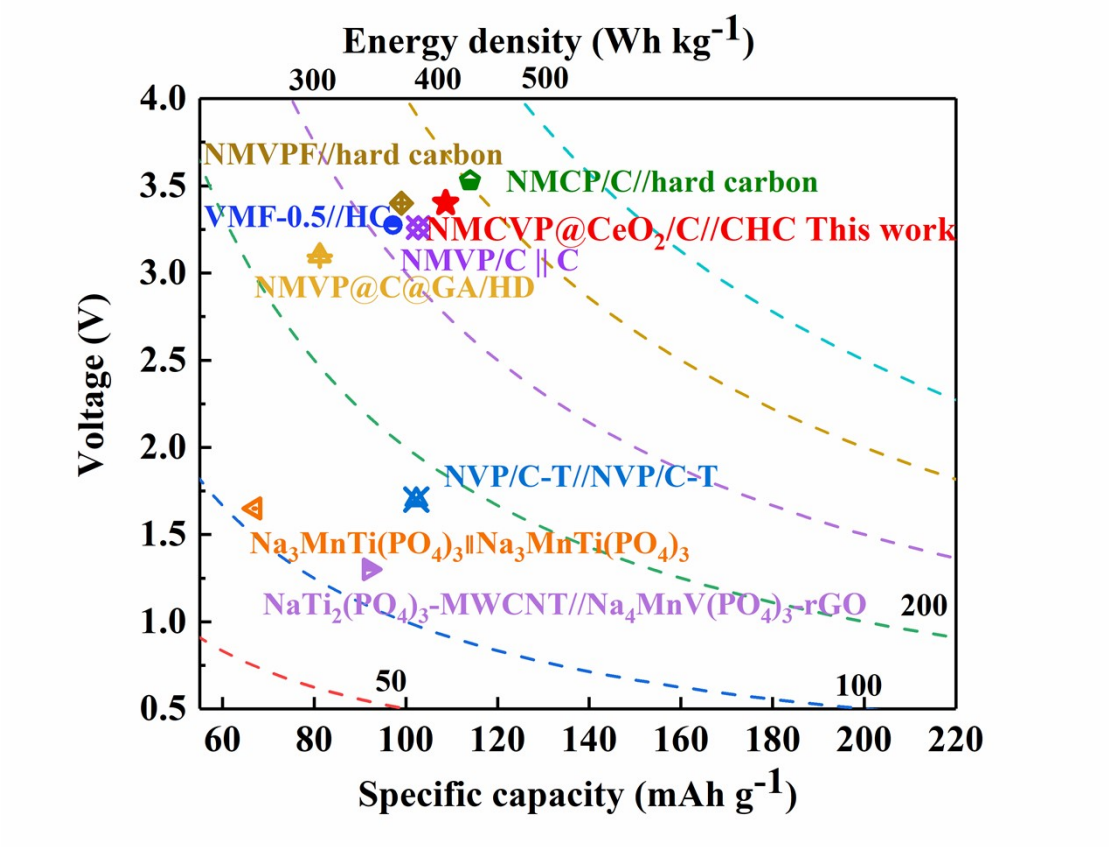


**Figure S10** (a) The comparison of voltage, capacity and energy density for the NMCVP@$CeO_2$/C//CHC full-cell with other recent reported sodium-ion full cell systems.

( NMVP@C@GA/HD[3], NVP/C-T//NVP/C-T[4], $NaTi_2(PO_4)_3$-MWCNT//NMVP-rGO[5], NMVP/C||C[6], NMCP/C//hard carbon[7], $Na_3MnTi(PO_4)_3$‖$Na_3MnTi(PO_4)_3$[8], NMVPF // hard carbon[9], VMF-0.5//HC[10])

**Table S1** Detailed structural information of $Na_4Mn_{1-x}Ce_xV(PO_4)_3/C$ (x = 0) from Rietveld refinement.

Space group R-3c

a= 8.94820Å b=8.94820Å c=21.54300Å

α=β=90.000° γ=120.000° V= 1493.854 Å$^3$

| atom | x | y | z | Mult. | Occupacy | Uiso |
|---|---|---|---|---|---|---|
| Na1 | 0.00000 | 0.00000 | 0.00000 | 6 | 1.0400 | 0.034 |
| Na2 | 0.64370 | 0.00000 | 0.25000 | 18 | 0.9710 | 0.026 |
| V | 0.00000 | 0.00000 | 0.14901 | 12 | 0.5000 | 0.031 |
| Mn | 0.00000 | 0.00000 | 0.14901 | 12 | 0.5000 | 0.021 |
| O1 | 0.01630 | 0.20970 | 0.19441 | 36 | 1.0000 | 0.027 |
| O2 | 0.18400 | 0.17690 | 0.08256 | 36 | 1.0000 | 0.020 |
| P1 | 0.29960 | 0.00000 | 0.25000 | 18 | 1.0000 | 0.034 |

**Table S2** Detailed structural information of $Na_4Mn_{1-x}Ce_xV(PO_4)_3/C$ (x = 0.05) from Rietveld refinement.

Space group R-3c

a= 8.94860Å b=8.94860Å c=21.55900Å

α=β=90.000° γ=120.000° V= 1495.097 Å$^3$

| atom | x | y | z | Mult. | Occupacy | Uiso |
|---|---|---|---|---|---|---|
| Na1 | 0.00000 | 0.00000 | 0.00000 | 6 | 1.0400 | 0.041 |
| Na2 | 0.64330 | 0.00000 | 0.25000 | 18 | 0.9710 | 0.0109 |
| V | 0.00000 | 0.00000 | 0.14901 | 12 | 0.5000 | 0.0109 |
| Mn | 0.00000 | 0.00000 | 0.14901 | 12 | 0.4500 | 0.0485 |
| Ce | 0.00000 | 0.00000 | 0.14901 | 12 | 0.0500 | 0.033 |
| O1 | 0.01730 | 0.21420 | 0.19396 | 36 | 1.0000 | 0.0266 |
| O2 | 0.18310 | 0.17800 | 0.08194 | 36 | 1.0000 | 0.0256 |
| P1 | 0.30240 | 0.00000 | 0.25000 | 18 | 1.0000 | 0.0345 |

**Table S3** Detailed structural information of $Na_4Mn_{1-x}Ce_xV(PO_4)_3/C$ (x = 0.1) from Rietveld refinement.

Space group R-3c

a= 8.95100Å b=8.95100Å c=21.55870Å

α=β=90.000° γ=120.000° V= 1495.879 Å$^3$ $CeO_2$%=1.25

| atom | x | y | z | Mult. | Occupacy | Uiso |
|---|---|---|---|---|---|---|
| Na1 | 0.00000 | 0.00000 | 0.00000 | 6 | 1.0400 | 0.028 |
| Na2 | 0.64250 | 0.00000 | 0.25000 | 18 | 0.9710 | 0.0089 |
| V | 0.00000 | 0.00000 | 0.14901 | 12 | 0.5000 | 0.01095 |
| Mn | 0.00000 | 0.00000 | 0.14901 | 12 | 0.4000 | 0.00052 |
| Ce | 0.00000 | 0.00000 | 0.14901 | 12 | 0.1000 | 0.281 |
| O1 | 0.01750 | 0.21690 | 0.19342 | 36 | 1.0000 | 0.01863 |
| O2 | 0.18630 | 0.17700 | 0.08175 | 36 | 1.0000 | 0.00760 |
| P1 | 0.29800 | 0.00000 | 0.25000 | 18 | 1.0000 | 0.02052 |

**Table S4** Detailed structural information of $Na_4Mn_{1-x}Ce_xV(PO_4)_3/C$ (x = 0.15) from Rietveld refinement.

Space group R-3c

a= 8.94140Å b=8.94140Å c=21.57440Å

α=β=90.000° γ=120.000° V= 1493.758 Å$^3$ $CeO_2$%=2.72

| atom | x | y | z | Mult. | Occupacy | Uiso |
|---|---|---|---|---|---|---|
| Na1 | 0.00000 | 0.00000 | 0.00000 | 6 | 1.0400 | 0.046 |
| Na2 | 0.64550 | 0.00000 | 0.25000 | 18 | 0.9710 | 0.0249 |
| V | 0.00000 | 0.00000 | 0.14901 | 12 | 0.5000 | 0.01095 |
| Mn | 0.00000 | 0.00000 | 0.14901 | 12 | 0.4000 | 0.40052 |
| Ce | 0.00000 | 0.00000 | 0.14901 | 12 | 0.1000 | 0.800 |
| O1 | 0.01800 | 0.20690 | 0.19251 | 36 | 1.0000 | 0.02663 |
| O2 | 0.18710 | 0.17990 | 0.08333 | 36 | 1.0000 | 0.03260 |
| P1 | 0.29790 | 0.00000 | 0.25000 | 18 | 1.0000 | 0.03752 |

**Table S5** Electronic conductivity of all composites.

| Sample | electronic conductivty (S/cm) |
|---|---|
| x=0 | $2.77\times10^{-3}$ |
| x=0.05 | $3.53\times10^{-3}$ |
| x=0.1 | $1.60\times10^{-2}$ |
| x=0.15 | $3.84\times10^{-3}$ |

**Table S6** comparison between NMCVP@$CeO_2$/C and other reported NMVP cathodes.

| Sample | Discharge capacity | Voltage range | Capacity retention | References |
|---|---|---|---|---|
| $\mathbf{Na_4Mn_{0.9}Ce_{0.1}V(PO_4)_3/C}$ | 121.2 mAh $g^{-1}$ at 0.2C<br>50.3 mAh $g^{-1}$at 50C | 2.5-3.8V | 91 mAh $g^{-1}$ at 0.2C for 2000$^{th}$ cycle (86.7% retention) | This work |
| $\mathbf{Na_{3.75}V_{1.25}Mn_{0.75}(PO_4)_3}$ | 102 mA h $g^{-1}$ at 0.2 C | 2.75-3.8V | 84.5 mA h $g^{-1}$ at 5C for 100$^{th}$ cycle (96% retention) | [11] |
| $\mathbf{Na_4VMn_{0.9}Cu_{0.1}(PO_4)_3/C}$ | 117 mA h $g^{-1}$ at 0.25 C<br>68 mA h $g^{-1}$ at 40 C | 2.4-3.8 V | 79 mA h $g^{-1}$ at 1C for 450 $^{th}$ cycle (90% retention) | [2] |
| $\mathbf{Na_{3.4}Mn_{0.4}Cr_{0.6}V(PO_4)_3}$ | Approximately 90 mA h $g^{-1}$ at 0.2 C | 2.0-4.3V | 63.1 mA h $g^{-1}$ at 5 C for 25 $^{th}$ cycle (70% retention) | [12] |
| $\mathbf{Na_xVMn_{0.75}Mg_{0.25}\ (PO_4)_3}$ | 78 mA h $g^{-1}$ at 1 C | 2.75-3.8V | 78 mA h $g^{-1}$ at 1C for 100 $^{th}$ cycle (96% retention) | [13] |
| $\mathbf{Na_xVMn_{0.75}Al_{0.25}(PO_4)_3}$ | 92 mA h $g^{-1}$ at 1 C | 2.75-3.8V | 92 mA h $g^{-1}$ at 1 C for 100 $^{th}$ cycle (96% retention) | [13] |
| $\mathbf{Na_4VMn_{0.5}Fe_{0.5}\ (PO_4)_3/C}$ | 120.0 mA h $g^{-1}$ at 0.5C | Rate performance 2.0-4.0V<br>Cycling performance 2.0-3.8V | 103.5 mA h $g^{-1}$ at 5 C for 500$^{th}$ cycle (99.3% retention) | [10] |

**Table S7** The difference of electric potential between anodic and cathode peaks for all the compositions

| Sample | 0 | 0.05 | 0.1 | 0.15 |
|---|---|---|---|---|
| $E_{A1}$ (V) | 3.226 | 3.249 | 3.239 | 3.226 |
| $E_{A2}$ (V) | 3.510 | 3.515 | 3.504 | 3.504 |
| $E_{C1}$ (V) | 3.484 | 3.473 | 3.452 | 3.454 |
| $E_{C2}$ (V) | 3.661 | 3.647 | 3.633 | 3.659 |
| $\Delta E_{A1-C1}$ | 0.258 | 0.224 | 0.213 | 0.228 |
| $\Delta E_{A2-C2}$ | 0.151 | 0.132 | 0.129 | 0.155 |

**Table S8** All the corresponding parameters acquired by EIS measurement

| Sample | $R_S$ (Ω/cm$^2$ ) | $R_{CT}$ (Ω/cm$^2$ ) | σ (Ω cm$^2$/s$^{-1/2}$) | D (cm$^2$/s) |
|---|---|---|---|---|
| x=0 | 5.04 | 309 | 72.58 | $2.81\times10^{-10}$-$10^{-11}$ |
| x=0.05 | 11.02 | 284.3 | 68.67 | $3.14\times10^{-11}$ |
| x=0.1 | 4.61 | 240.1 | 32.23 | $1.42\times10^{-10}$ |
| x=0.15 | 5.46 | 357.3 | 57.66 | $4.45\times10^{-11}$ |

**References:**


[1] W. Zhang, Z. Zhang, H. Li, D. Wang, T. Wang, X. Sun, J. Zheng, Y. Lai, Engineering 3D Well-Interconnected $Na_4MnV(PO_4)_3$ Facilitates Ultrafast and Ultrastable Sodium Storage, Acs Appl Mater Inter 11 (2019) 35746-35754.

[2] V. Soundharrajan, M. H. Alfaruqi, S. Lee, B. Sambandam, S. Kim, S. Kim, V. Mathew, D. T. Pham, J. Hwang, Y. Sun, J. Kim, Multidimensional $Na_4VMn_{0.9}Cu_{0.1}(PO_4)_3$/C Cotton-Candy Cathode Materials for High Energy Na-ion Batteries, J. Mater Chem a 8 (2020) 12055-12068.

[3] H. Li, T. Jin, X. Chen, Y. Lai, Z. Zhang, W. Bao, L. Jiao, Rational Architecture Design Enables Superior Na Storage in Greener NASICON-$Na_4MnV(PO_4)_3$ Cathode, Adv Energy Mater 8 (2018) 1801418.

[4] R. Ling, S. Cai, D. Xie, X. Li, M. Wang, Y. Lin, S. Jiang, K. Shen, K. Xiong, X. Sun, Three-Dimensional Hierarchical Porous $Na_3V_2(PO_4)_3$/C Structure with High

Rate Capability and Cycling Stability for Sodium-Ion Batteries, Chem. Eng. J. 353 (2018) 264-272.

[5] P. Ramesh Kumar, A. Kheireddine, U. Nisar, R. A. Shakoor, R. Essehli, R. Amin, I. Belharouak, $Na_4MnV(PO_4)_3$-rGO as Advanced Cathode for Aqueous and Non-Aqueous Sodium Ion Batteries, J. Power Sources 429 (2019) 149-155.

[6] X. Ma, X. Cao, Y. Zhou, S. Guo, X. Shi, G. Fang, A. Pan, B. Lu, J. Zhou, S. Liang, Tuning Crystal Structure and Redox Potential of NASICON-type Cathodes for Sodium-Ion Batteries, Nano Res 13 (2020) 3330-3337.

[7] J. Zhang, Y. Liu, X. Zhao, L. He, H. Liu, Y. Song, S. Sun, Q. Li, X. Xing, J. Chen, A Novel NASICON-Type $Na_4MnCr(PO_4)_3$ Demonstrating the Energy Density Record of Phosphate Cathodes for Sodium-Ion Batteries, Adv. Mater. 32 (2020) 1906348.

[8] Y. Zhou, X. Shao, K. Lam, Y. Zheng, L. Zhao, K. Wang, J. Zhao, F. Chen, X. Hou, Symmetric Sodium-Ion Battery Based on Dual-Electron Reactions of NASICON-Structured $Na_3MnTi(PO_4)_3$ Material, Acs Appl Mater Inter 12 (2020) 30328-30335.

[9] J. Hou, M. Hadouchi, L. Sui, J. Liu, M. Tang, W. H. Kan, M. Avdeev, G. Zhong, Y. Liao, Y. Lai, Y. Chu, H. Lin, C. Chen, Z. Hu, Y. Huang, J. Ma, Unlocking Fast and Reversible Sodium Intercalation in NASICON $Na_4MnV(PO_4)_3$ by Fluorine Substitution, Energy Storage Materials 42 (2021) 307-316.

[10] C. Xu, J. Zhao, E. Wang, X. Liu, X. Shen, X. Rong, Q. Zheng, G. Ren, N. Zhang, X. Liu, X. Guo, C. Yang, H. Liu, B. Zhong, Y. S. Hu, A Novel NASICON-Typed $Na_4VMn_{0.5}Fe_{0.5}(PO_4)_3$ Cathode for High-Performance Na-Ion Batteries, Adv Energy Mater 11 (2021) 2100729.

[11] S. Ghosh, N. Barman, M. Mazumder, S. K. Pati, G. Rousse, P. Senguttuvan, High Capacity and High-Rate NASICON-$Na_{3.75}V_{1.25}Mn_{0.75}(PO_4)_3$ Cathode for Na-Ion Batteries via Modulating Electronic and Crystal Structures, Adv Energy Mater 10 (2019) 1902918.

[12] P. Lavela, R. Klee, J. L. Tirado, On the Benefits of Cr Substitution On $Na_4MnV(PO_4)_3$ to Improve the High Voltage Performance as Cathode for Sodium-Ion

Batteries, J. Power Sources 495 (2021) 229811.

[13] S. Ghosh, N. Barman, P. Senguttuvan, Impact of $Mg^{(2+)}$ and $Al^{(3+)}$ Substitutions On the Structural and Electrochemical Properties of NASICON-$Na_xVMn_{0.75}M_{0.25}(PO_4)_3$ (M = Mg and Al) Cathodes for Sodium-Ion Batteries, Small 16 (2020) e2003973.